摘要

制备了一种以 PCL，PHEMA 聚合物为疏水组分，PMEO2MA 为亲水组分的新型梳状高分子。该高分子具有特殊的侧链结晶效应，有利于在组装过程中减小粒子间距。以该高分子为模板能制备出由 6 nm 的 AuNP 组成纳米链，该纳米链经过进一步的亲疏水自组装过程，最终形成了在近红外区域光吸收性能良好的金粒子胶束（Gold NM），该胶束结构不仅能用于光热治疗，还同时具备光控释放疏水药物，CT 造影，光声成像等功能，能应用于多功能成像和光热疗-化疗联合治疗，在细胞实验和动物实验上都展现了良好效果。值得一提的是，在该胶束结构在生理条件下能降解为 6 nm 的金球，顺利从体内代谢出去。

Theranostic Gold Nanomicelles made from Biocompatible Comb-like Polymers for Thermochemotherapy and Multifunctional Imaging with Rapid Clearance

*Heng Deng, Fengying Dai, Guanghui Ma, and Xin Zhang**

Multifunctional nanomaterials with combined diagnostic and therapy functions have emerged as a promising tool for imaging and tumor treatment in personalized biomedical applications.[1] However, it is still a challenge to obtain one single nano platform with coordinated functions of diagnostics and therapy. Hybrid gold nanoparticle (AuNP) aggregations, which exploit the merits of both inorganic nanomaterial and polymer, have emerged as a new paradigm for multimodality theranostic applications in cancer treatment.[2] These gold nanostructures are assembled from linear amphipathic-polymer-coated AuNPs, which inherit the self-assembly ability of the amphipathic polymers and can form special 3D structures. On the one hand, the introduction of AuNPs secures the whole system with special physical properties, like surface plasmon resonance (SPR) and high mass attenuation coefficient, which can be used for photothermal therapy (PTT)/photoacoustic tomography (PAT) and X-ray computed tomography (CT) imaging,[2b,3] respectively. On the other hand, polymer not only offers the drive to tune the plasmonic response of AuNPs aggregations, which can transfer AuNPs into near infrared (NIR) photothermal conversion reagents, but also can be used as drug carrier for on-demand drug release under NIR laser stimulate.[4] Some pioneering and interesting research work has been done in this field. In particular, Chen used PS-PEG coated 40 nm AuNPs or PCL-PEG-coated 26 nm AuNPs as building blocks to obtain gold vesicles that showed a SPR peak in NIR region for PTT agents and PAT probes.[2b,5] Duan used PMMA/PEG mixed grafted 14 nm AuNPs to construct gold superstructures as carriers for drug delivery.[5] Our recent study also revealed that large compound micelles made by PCL/$PMEO_2MA$-grafted 14 nm AuNPs successfully served as theranostic agents for NIR PTT and CT imaging.[3]

Even though gold is extraordinarily biocompatible, AuNPs may have size-dependent toxicity to animals. Huang found that AuNPs ranging from 8 to 37 nm (core size) induced severe sickness in mice, but AuNPs smaller than 8 nm would not induce sickness or lethality in mice.[6] Thus, an ideal hybrid AuNPs aggregation is expected to harbor the following two features: i) the diameter of the noble-metal nanoparticle should be less than 8 nm, which reduces its potential toxicity. ii) A strong absorption in the NIR region, in which lasers feature high penetrability into the skin, resulting in less damage.[7] However, the building block AuNPs used by these research papers were all bigger than 8 nm. Considering the fact that the LSPR phenomenon of AuNPs is related to the value of d/D (distance between AuNPs/diameter of AuNPs), the smaller AuNPs we use as the building block, the more difficult we tune them into strong NIR photoabsorber.[5,8] Therefore, the self-assembly of small AuNPs with diameters of less than 8 nm that realize PAT/CT imaging, chemotherapy, and hyperthermia in a coordinated way would be a challenge.

To find the breach of this challenge, we tried to replace the linear polymer with better designed multi-mercapto-terminated comb-like amphipathic polymer to modify and self-assemble AuNPs. The comb-like polymer is a novel special type of graft copolymer with unique side-chain crystallization phenomenon which is beneficial for reducing the distance between adjacent AuNPs during the assembly process.[9] In addition, the comb-like polymer will play dual role on forming AuNPs aggregations: i) in the first stage, the multi-mercapto-terminated group could bond more than one AuNPs on a single polymer forming a hybrid AuNPs/polymer structure; ii) based on the first stage, this hybrid AuNPs/polymer structure could further self-assemble by hydrophilic/hydrophobic interactions. With the dual-modal driving force of multi-mercapto cross binding and hydrophilic/hydrophobic interaction, smaller 8 nm AuNPs could be tightly packed which enhanced electromagnetic coupling of adjacent AuNPs and greatly improves the absorbance of AuNPs in the NIR region.

Herein, we developed a novel comb-like amphipathic polymer composed of biodegradable hydrophobic poly(ε-caprolactone) (PCL)/poly(2-hydroxyethyl methacrylate) (PHEMA) and hydrophilic poly[2-(2-methoxyethoxy) ethyl methacrylate] ($PMEO_2MA$),[10] and employed this polymer to assist assembling DOX@gold nanomicelles (DOX@Gold NMs), which showed strong absorbance in the NIR region, for multimodal bioimaging and highly effective in vivo chemotherapy and photothermal therapy of tumors in mouse model. While exhibiting no obvious toxicity to cells, our gold NMs could serve as a powerful photothermal agent and drug carrier that could effectively kill cancer cells in vitro under NIR laser irradiation. Due to the

H. Deng, Prof. F. Dai, Prof. G. Ma, Prof. X. Zhang
National Key Laboratory of Biochemical Engineering
Institute of Process Engineering
Chinese Academy of Sciences
Beijing 100190, PR China
E-mail: xzhang@ipe.ac.cn

H. Deng
School of Chemistry and Chemical Engineering
University of Chinese Academy of Sciences
Beijing 100049, PR China

DOI: 10.1002/adma.201501420

intense X-ray attenuation ability and high NIR optical absorbance of gold NMs, obvious tumor contrasts could be observed by CT and PAT bimodal imaging in vivo. Highly effective in vivo combined photothermal-chemotherapy of tumors is finally achieved, with a low dose of DOX@Gold NMs and a low power density of an NIR laser, realizing nearly 100% of tumor elimination after combined therapy. In addition, gold NMs could be decomposed into 6 nm AuNPs which guaranteed the safety of the gold NMs and their clearance from the body. Therefore, our work highlights new possibilities of using comb-like amphipathic polymer for assembling small AuNPs into strong NIR absorption nanostructures for biomedical applications such as cancer imaging and therapy as shown in **Figure 1**A, and encourages further in-depth investigations of this novel type of 3D gold nanomaterials for biomedical applications.

We used reversible addition-fragmentation chain transfer polymerization (RAFT) and ring-opening polymerization (ROP) to synthesize the comb-like polymer *p*-(MEO_2MA-*co*-(HEMA-*g*-PCL)) in two-step approach as shown in Figure S1, Supporting Information: i) the backbone polymer *p*-(MEO_2MA-*co*-HEMA) was first synthesized by RAFT; ii) the comb teeth polymer PCL was grafted from *p*-(MEO_2MA-*co*-HEMA) by ROP. The chemical composition of the obtained polymer was studied by ^1H NMR spectroscopy (Figure S2, Supporting Information), which suggested the successful synthesis of the comb-like polymer.[10a,11] To endow the polymer with excellent reaction ability with gold particles, the mercapto group was introduced at the OH group of the PCL according to a published protocol.[12] In order to make it clear that different hydrophilic/hydrophobic ratios of polymer would influence the assembly of AuNPs, a series of comb-like polymers with different hydrophilic/hydrophobic ratios was synthesized as listed in Table S1, Supporting Information. Under these polymers' assistance, a series of gold AuNP aggregation structures (Figure S3, Supporting Information) could be obtained with different NIR absorbance abilities and hydrodynamic sizes (Figure S4 and S5, Supporting Information), and the higher hydrophobic/hydrophilic ratios guaranteed better NIR absorbance ability with bigger hydrodynamic size. By balancing the ability to absorb NIR laser irradiation and the size of the gold assembly, the gold nanomicelles made by the polymer *p*-(MEO_2MA_{270}-*co*-(HEMA-*g*-PCL_{25})$_{260}$) were chosen for further exploration.

Gold NMs were prepared under the assistance of our smart comb-like polymer as shown in Figure 1a. In order to obtain AuNPs smaller than 8 nm, we adopted the $NaBH_4$ reduction method, which was used to produce gold seeds.[13] The comb-like polymer played important roles in stabilizing the as-synthesized AuNPs: a huge size aggregation would be formed without the presence of polymer (Figure S6, Supporting Information). In the presence of comb-like polymer, $HAuCl_4$ was reduced by $NaBH_4$ in *N,N*-dimethylformamide (DMF) while forming chain-like structures composed of small 6.1 ± 1.8 nm AuNPs (inset in Figure 1B(I)), as shown in Figure 1B(I). The chains comprised bifurcated junctions, which were often interconnected to obtain a branched network. The formation of chain structures could be attributed to the multi-mercapto-terminated groups of the comb-like polymer that bound the AuNPs together, resulting in a distance reduction between the nanoparticles, which showed a 60 nm red-shift of LSPR peak compared to discrete AuNPs (Figure 1C). Because our comb-like polymer was composed of hydrophilic and hydrophobic parts, the as-synthesized gold chains could further assemble by hydrophilic/hydrophobic interactions.[2b] By dialyzing the DMF solution of a gold chain against water, the assembly process of the gold chains would take place as shown in Figure 1B(II)–(V). With dialysis time expansion and water content increasing, the hydrophobic brush PCL collapsed on the surface of the AuNPs to minimize the overall free energy,[2b,5] which could drive the gold chains to curl up into small loop aggregations (Figure 1B(II)). In order to further reduce the free energy of system, small loop aggregations were inclined to aggregate together (Figure 1B(III)) which gradually formed from a loosely packed compound micelle (Figure 1B(IV)) to a 300 nm tightly packed compound micelle (Figure 1B(V)); due to the strictly packed micelles being aggregated from short gold chains, their LSPR centered at 800 nm (Figure 1C), which belonged to the NIR region. An ultrathin cross-section TEM image was also taken to investigate the inner structure of these gold NMs, which showed that the interior of the gold NMs was solid and almost full of short gold chains (Figure 1D). Compared with our recent work on 500 nm gold large compound micelle composed of 14 nm AuNPs,[3] these new gold NMs make progress on two points: the smaller overall size (about 300 nm) and smaller building blocks size (about 6 nm). These improvements might be contributed to the following reasons: i) the comb-like polymer possessed the side-chain crystallization phenomenon, which was beneficial for reducing the distance between adjacent AuNPs; ii) the building blocks of the self-assembly process were in fact gold chains, which had already showed red-shift of LSPR peak (Figure 1C). In addition, according to the TGA measurement, our gold NMs possessed about 20% (Figure S7, Supporting Information) polymer, this part of the polymer could be a vessel for a hydrophobic drug such as DOX. By mixing hydrophobic DOX and gold chains in DMF and dialyzing against water, the DOX could be packaged into the gold NMs, with a loading content of 5% (if only the weight of the polymer was counted, the loading content could reach to about 20.7%).

In order to investigate the photothermal properties of our materials, gold NMs with different concentrations were exposed to 808 nm NIR laser at a power density of 1.5 W cm^{-2}, which is a moderate power in common use.[1a,1b] With the concentration of gold NMs increasing from 0.1 and 0.2 mg mL^{-1} to 0.4 mg mL^{-1}, the final temperature of solution could reach 40, 57, and 71 °C by laser irradiation for 5 min, respectively, while pure water showed negligible temperature change (Figure 1E). The TEM images before and after laser irradiation were also taken, which suggested the tightly packed gold NMs tended to dissociate after laser irradiation (Figure 1F). This phenomenon has been reported in several research papers,[2b,4,14] that the sort of gold aggregations driven by the amphipathic polymer were unstable under laser irradiation, which could be used for on-demand release of drugs under the stimulus of a laser.

As materials being used in biomedicine, safety should be put into first consideration. In this sense, we first tested the potential toxicity of our gold NMs (without DOX) to Michigan Cancer Foundation-7 (MCF-7) cells, murine fibroblasts (L929) cells, and human umbilical endothelial vein cells (HUEVC) by standard methyl thiazolyl tetrazolium (MTT) assay. Even after

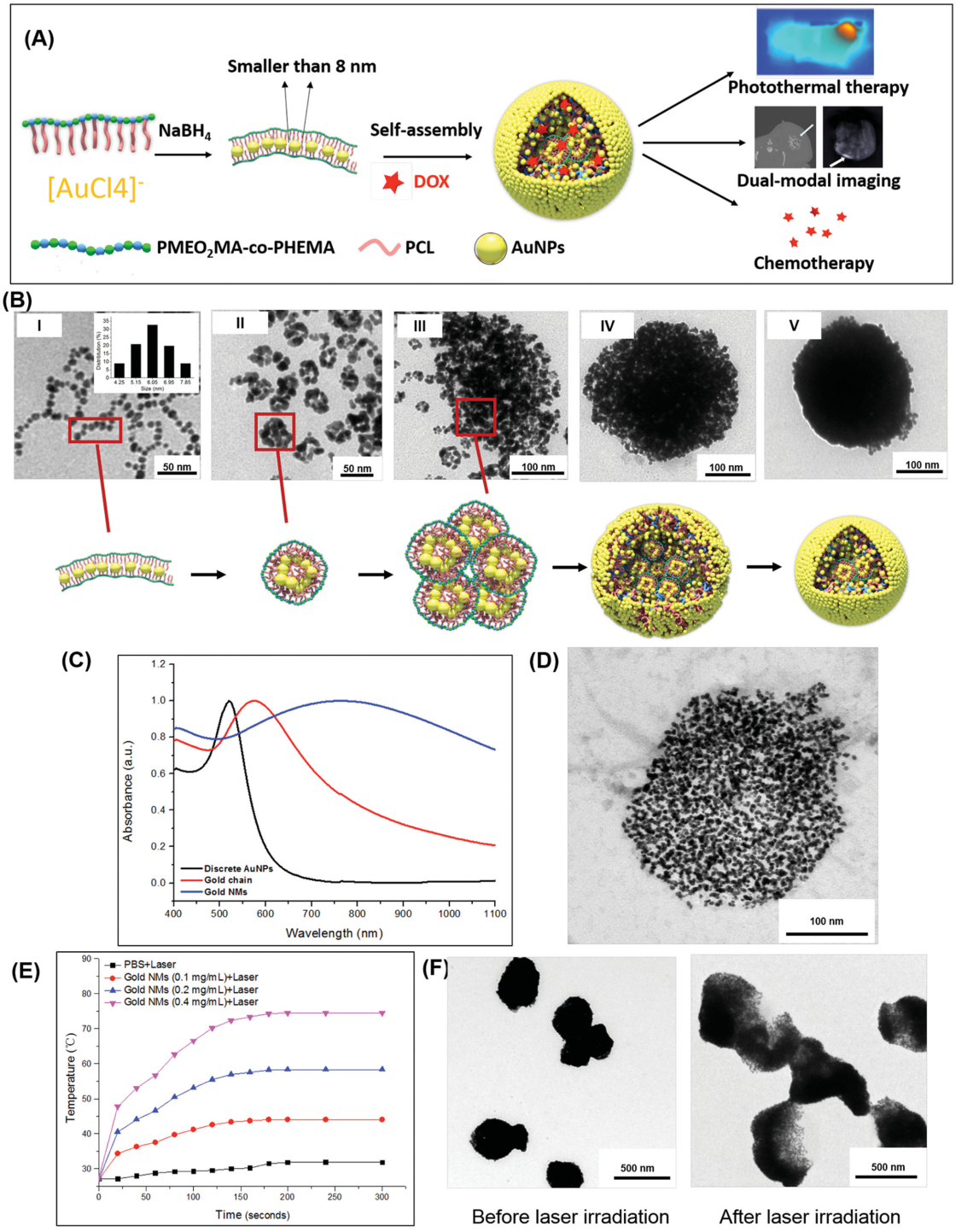

Figure 1. Gold NM synthesis and characterization. A) Schematic representation of synthesis of DOX@Gold NMs and their potential theranostic application. B) TEM images and schematic pictures showing the assembly process of Gold NMs: (I) gold chain composed by 6.1 ± 1.8 nm AuNPs in DMF (the inset showing the size distribution of AuNPs); (II), (III), (IV), and (V) the self-assembly stage at different dialysis times (0.1, 2, 6, and 12 h, respectively). C) UV–vis–NIR absorbance spectra of 6 nm AuNPs (black line), gold chain composed of 6.1 ± 1.8 nm AuNPs (red line), and gold NMs made from 6.1 ± 1.8 nm AuNPs (blue line). D) Ultrathin cross-section TEM images showing the interior structure of the gold NMs. E) The photothermal heating curves of pure water and gold NM solutions with different concentrations (0.1, 0.2, and 0.4 mg mL^{-1}) under 808 nm laser irradiation at the power density of 1.5 W cm^{-2}. F) TEM images of the gold NMs before and after laser irradiation.

incubating with gold NMs at high concentrations of 2 mg mL^{-1} for 24 h, these three types of cells still remained at a high cell viability of above 80% (**Figure 2**A and Figure S8, Supporting Information), which demonstrated the safety of our nanomaterials. Considering that the main components of our gold nanomicelles (PCL, PHEMA, $PMEO_2MA$, and AuNPs) are

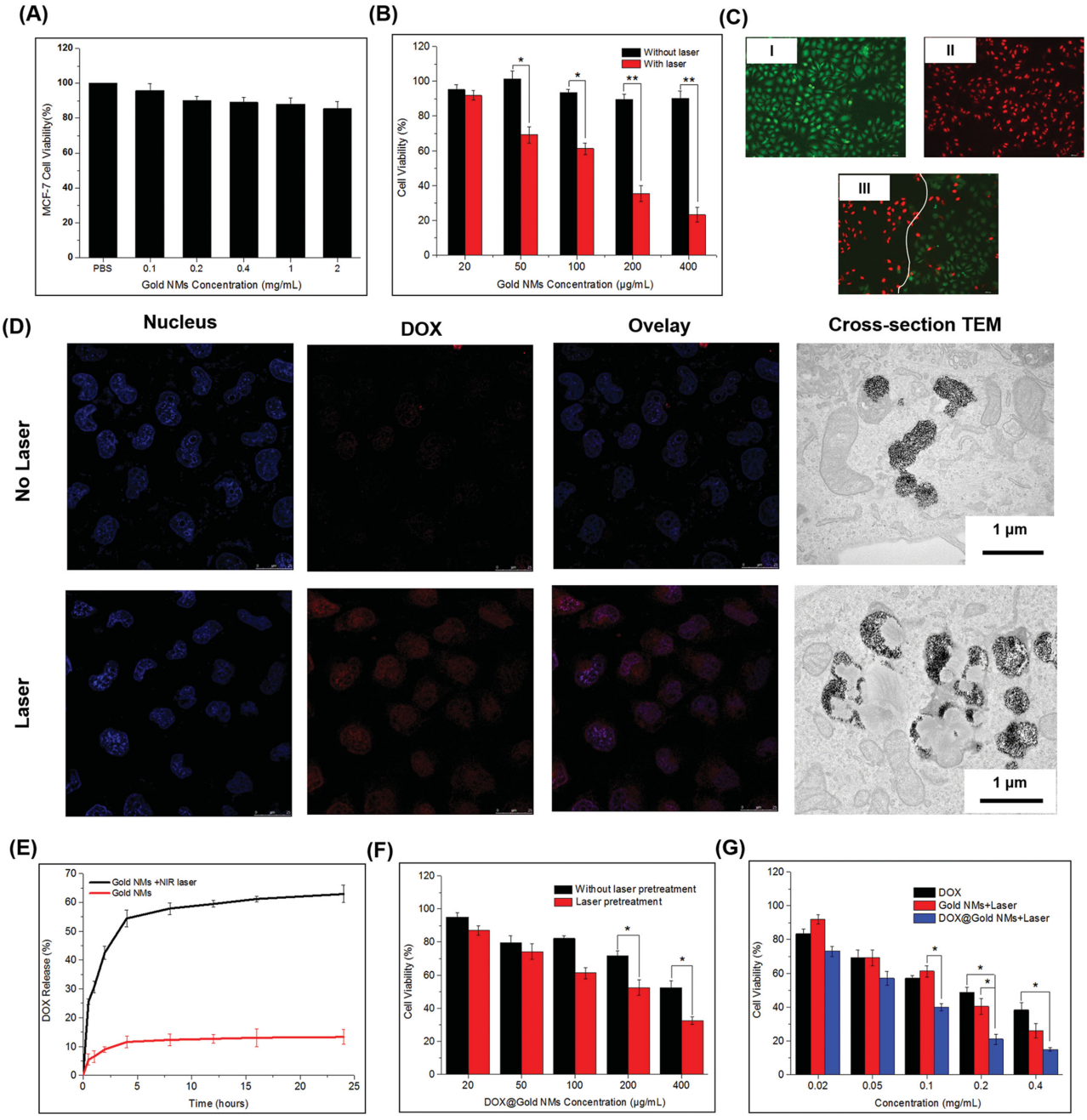

Figure 2. In vitro cell experiments. A) Relative viabilities of MCF-7 cells after being incubated with different concentrations of Gold NMs (0.1, 0.2, 0.4, 1.0, and 2.0 mg mL^{-1}) for 24 h. B) MCF-7 cell relative viability incubated with different concentration of gold NMs (0.02, 0.05, 0.1, 0.2, and 0.4 mg mL^{-1}) for 4 h at 37 °C, then the cells were illuminated using a 808 nm laser (1.5 W cm^{-2}, 5 min). C) Fluorescence images of Calcein AM and PI co-stained cancer cells: (I) without Gold NMs (laser only), (II) incubated with gold NMs at the center spot of laser irradiation, (III) incubated with Gold NMs at the edge of laser spot. D) Confocal microscopy images and ultrathin cross-section TEM images of cell incubated with DOX@gold NMs (pretreated with laser and no laser). E) NIR-triggered release of DOX from Gold NMs, the samples were irradiated with an NIR laser (1.5 W cm^{-2}) for 5 min. F)relative viabilities of MCF-7 incubated with DOX@gold NMs (with or without the pretreatment of NIR laser irradiation) of different concentrations (0.02, 0.05, 0.1, 0.2, and 0.4 mg mL^{-1}) for 24 h. G) Relative viabilities of different groups of MCF-7 after various treatments (DOX only, gold NMs + laser, DOX@gold NMs + laser), the free DOX group used an equivalent DOX concentration to the DOX@gold NMs group. $*P < 0.05$, $**P < 0.01$.

all biocompatible, the low cytotoxicity of our materials was a matter of course.[2b,10] Next, we used gold NMs as the photothermal agent for in vitro MCF-7 cell ablation under 808 nm laser irradiation. First, MCF-7 cells were incubated with gold NMs at different concentrations for 4 h and then irradiated by the 808 nm laser. Even though the sizes of these gold NMs were about 300 nm, they could still get into the cells, as shown by the ultrathin cross-section TEM image of the MCF-7 cells

incubated with gold NMs (Figure S9, Supporting Information). Following laser irradiation, MTT assay was performed to quantitatively measure the relative cell viabilities after PTT treatment with different concentrations of gold NMs, and concentration-dependent cytotoxicity to MCF-7 cells was observed (Figure 2B). The cells were also stained by Calcein AM and propidium iodide (Figure 2C) to differentiate live cells (green) from dead ones (red), which indicated the PTT treatment was highly selective and localized.

As mentioned above, due to the tightly packed structure of micelle, hydrophobic DOX could be loaded into the gold micelles with negligible leakage of DOX before laser irradiation, as shown in confocal microscopy images (Figure 2D) and drug release curves (Figure 2E). When DOX was restrained inside of the gold NMs in which AuNPs had a fluorescence quenching effect on DOX,[15] nearly no red fluorescence of DOX could be observed in the no-laser-treated group (Figure 2D), which was agreement with the drug release result (Figure 2E). After laser irradiation, the gold NMs engulfed by cells became fragmented compared to the structure before laser irradiation, as shown in the ultrathin cross-section TEM image (Figure 2D), which was also agreement with the above TEM results (Figure 1F), and the drug release rate could reach about 60% (Figure 2E). The controllable on-demand release of DOX under laser irradiation was also demonstrated by confocal microscopy images (Figure 2D), in which, only after laser irradiation, DOX could release from the gold NMs and get rid of the fluorescence quenching effect of the AuNPs while showing a strong red fluorescence.[15] When DOX was released from the gold NMs under laser irradiation, the DOX concentration in the inner or surrounding microenvironment of cancer cells increased, which resulted in enhanced cytotoxicity to tumor cells. As shown in Figure 2F, the DOX@Gold NMs with laser pretreatment showed more remarkable chemotherapy effect than the control group. All the results demonstrated that gold NMs could be used as a drug carrier for releasing drug under the remote control of an NIR laser.

Because of the combined function of PTT agent and drug carrier, our gold NMs offered a good platform for combined photothermal-chemotherapy, which synergistically enhanced the tumor cell killing effect. As shown in the MTT result (Figure 2G), either chemotherapy (DOX) or photothermal therapy (gold NMs + laser group) alone could not achieve ideal results against tumor cells. By combining these two different therapies, cell viability decreased to 20% in the DOX@Gold NMs (0.2 mg mL^{-1}) + laser group (Figure 2G), which was better than either DOX treatment (cell viability was 45%) or PTT treatment (cell viability was 39%) alone (Figure 2G). These results revealed that the combination of chemotherapy and photothermal therapy through DOX@Gold NMs greatly increased the cell killing ability, which was explained by the synergistic reinforcement effect by each other, making it a promising approach for cancer therapy.[16]

Followed by the in vitro testing of the DOX@Gold NMs, we then investigated the feasibility of using the DOX@Gold NMs in MCF-7 tumor bearing mice. The agent dosage (2 mg mL^{-1}, 50 μL) was selected to ensure sufficient agent concentration in the tumor region, which was also a moderate dosage in intratumor injection.[1e,3,5] In order to clearly demonstrate the excellent photothermal effect of the gold NMs in vivo, a photothermal camera was used to record the temperature change as shown in **Figure 3**A. Upon irradiation by the 808 nm laser with a low power density of 1.5 W cm^{-2} for 5 min, the local tumor temperature of mice treated by gold NMs could rapidly increase to 62 °C (Figure 3B), which exceeds the damage

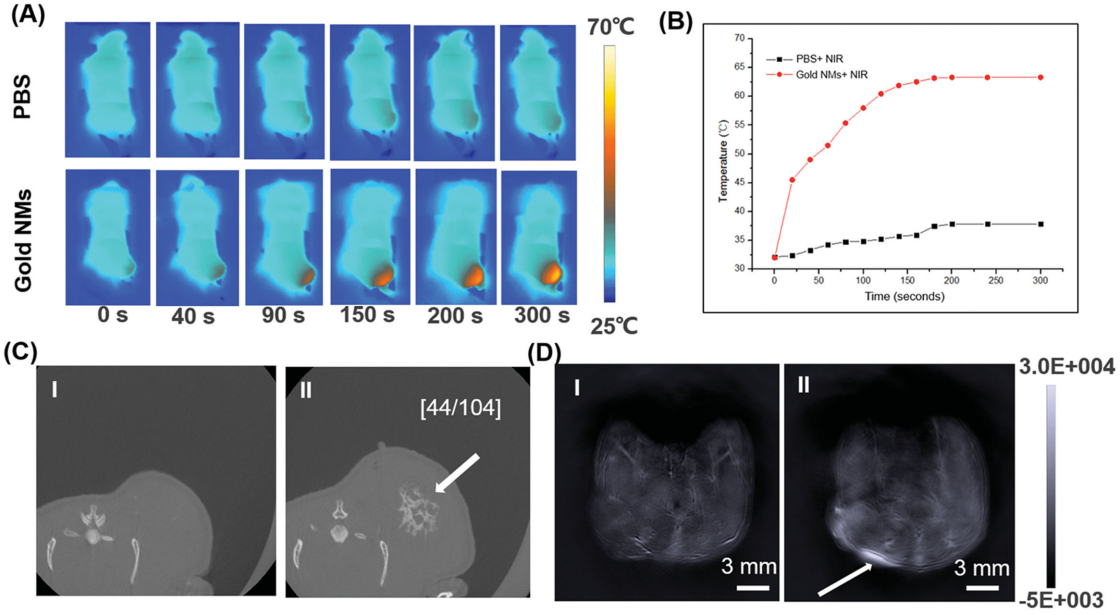

Figure 3. In vivo imaging in MCF-7 bearing mice. A) Thermal images of MCF-7 tumor-bearing mice exposed to irradiation from an 808 nm laser for 5 min after the injection of PBS (50 μL) and gold NMs (2 mg mL^{-1}, 50 μL); B) Heat curves of tumors upon laser irradiation as a function of irradiation time. C) CT images of mice before (I) and after (II) injection with gold NMs (2 mg mL^{-1}, 50 μL), the numbers in brackets are the HU values of the surrounding tissue (44) and the tumor site (104). D) PAT images of mice before (I) and after (II) injection with gold NMs (2 mg mL^{-1}, 50 μL). The arrows indicate the location of tumor.

threshold necessary.[17] In contrast, the local tumor temperature of the PBS control group only increased to 38 °C, suggesting that the low-power NIR laser was harmless to organs, which exhibited no killing effect to tumor. Encouraged by the in vivo photothermal effect of the gold NMs, PAT imaging was also employed in which contrast agents should be excellent light-absorbers.[18] In addition, the gold NMs were composed of gold nanomaterials, which have a strong ability to absorb and weaken the incident X-rays to produce tissue contrasts,[2b,19] therefore the dual-modal PAT/CT imaging could be realized by using our gold NMs as contrast agents. In our experiment the gold NMs were intratumorally injected in tumors: the gold concentration in the tumor region was high enough to distinguish tumors on the gold-enhanced CT image or PAT image with good contrast. According to a previous study,[2b,19] both these imaging technologies would produce an enhanced positive-contrast picture that could identify the tumor region from the surrounding region clearly. Before injection of gold NMs, the Hounsfield Units (HU) value and photoacoustic signal intensity of tumor region was low which was difficult to identify from surrounding tissues. After injection of Gold NMs, the HU value and photoacoustic signal intensity of tumor region could reach as high as 104 and 3.0×10^4, respectively (Figure 3C,D), which was markedly higher than those of surrounding tissues. Figure 3C,D demonstrated a good contrast enhancement between the tumor and the surrounding normal tissue after injection of gold NMs in both CT imaging and PAT imaging.

The antitumor efficiency of DOX@Gold NMs for photothermal-chemotherapy was also studied in MCF-7 tumor-bearing nude mice. To evaluate the therapeutic outcome, relative tumor volumes (V/V_0) were recorded (**Figure 4**A). In PBS, gold-NMs and laser-treated groups, tumors grew rapidly, and the highest relative tumor volume (V/V_0) could be as high as about 6 within 20 d. Tumors of the mice that were treated with DOX increased 3.5 times over 20 d, suggesting the low dosage of administered DOX in this study could not effectively inhibit the growth of tumors. As for the groups that received photothermal therapy and photothermal-chemotherapy, tumors treated with particles under laser irradiation could be effectively ablated, leaving black scars at the tumor sites as shown in Figure 4B. In the group that received only photothermal therapy, the tumor size maintained at the initial level and the scar could not be totally healed up (Figure 4B). Moreover when the mice were sacrificed for further anatomypathology research, we could find that a small size tumor was still under the scars (Figure S10, Supporting Information), showing that the purely photothermal therapy in this study could not totally clean up the tumors. As expected, when chemotherapy and photothermal therapy were combined together, the tumor size continued to diminish and the scars could totally coalesce finally (Figure 4B), leaving nearly no tumors under the skin (Figure S10, Supporting Information).The mice in photothermal-chemotherapy group were tumor-free after treatment and all survived over 40 d, while in the control groups, the mice showed relatively short life spans (Figure 4C). The therapeutic effect was also further demonstrated by hematoxylin and eosin (H&E) staining of tumors harvested from experimental animals. As shown in Figure S11, Supporting Information, the tumor cells of the photothermal-chemotherapy group received more-severe damage than the tumor cells from purely chemotherapy or photothermal therapy groups. Overall the results demonstrated that the combined DOX and photothermal treatment were more effective than either treatment alone. This exciting result might be attributed to following reasons. First, gold NMs as drug carriers could effectively enhance the local concentration of DOX in tumor cells to exhibit better cell-killing ability. Second, the hyperthermia effect by photothermal therapy would modulate the drug-resistance related genes and greatly enhance the sensitivity of the tumor cells toward chemotherapeutics.[16a]

Despite no obvious in vitro toxicity of the gold NMs to MCF-7 cell lines, as materials used in living body, its potential in vivo toxicity to animals should be also put into consideration.

Our gold NMs could be decomposed by laser irradiation as shown above (Figure 1F and Figure 2D), and the biocompatible coating polymer could be hydrolyzed in physiological conditions, which further facilitated the dissociation of the gold NMs.[2b,3] The TEM images of tumor, liver, and spleen (Figure S12, Supporting Information) showed that the gold NMs had been decomposed into 6 nm AuNPs. These 6 nm AuNPs induced no sickness or lethality in mice as shown in the anatomypathology research, in which no detectable lesions were observed for mice after treatment with gold NMs for 20 d from the H&E results (Figure S13, Supporting Information). Within 20 d after injection with gold NMs, no abnormalities in body weight were observed (Figure S14, Supporting Information) and the mice maintained normal behavior. These results were agreement with Huang's research that AuNPs less than 8 nm would show no toxicity to animals.[6] We also investigated the biodistribution of 6 nm AuNPs which had been dissociated from the gold NMs. There are some reports suggesting that when nanoparticles are small enough, they can be effectively cleared from body through the renal excretion route.[20] In light of this, we investigated particle tracking of gold NMs after intratumoral injection to see if these dissociated 6 nm AuNPs could be effectively cleared by urine. The amounts of the gold nanomaterials accumulated in the vital organs and vital metabolic products (bile, urine, and faeces) were quantified by ICP-MS measurements at different times (Figure 4D). We found a 4% dose of elemental Au was cleared from urine on day 7. This might be attributed to the following reason: 6 nm is near to the upper limit for renal clearance,[20] which was not so suitable for renal clearance. Figure 4D shows that gold NMs accumulated prominently in the reticuloendothelial system (RES) including the liver and the spleen on day 2, and then were cleared from the RES on day 7 (Figure 4D). These results indicate that gold NMs could be dissociated into 6 nm AuNPs after laser irradiation and under the physiological conditions over time, and these small AuNPs were nontoxic with reasonable clearance, which guaranteed the safety of using the gold NMs.

In summary, we have successfully developed a new generation of photothermal theranostic agents based on assembling 6 nm AuNPs by using novel comb-like amphipathic polymer as template. It is found that gold NMs exhibit good biocompatibility and show no observable toxicity to MCF-7, L929, and HUEVC, and can be used as a highly effective photothermal agent in vitro. Moreover, due to the special 3D structure of gold NMs, it could also be used as carriers for on-demand release of hydrophobic drug such as DOX. By combining chemotherapy

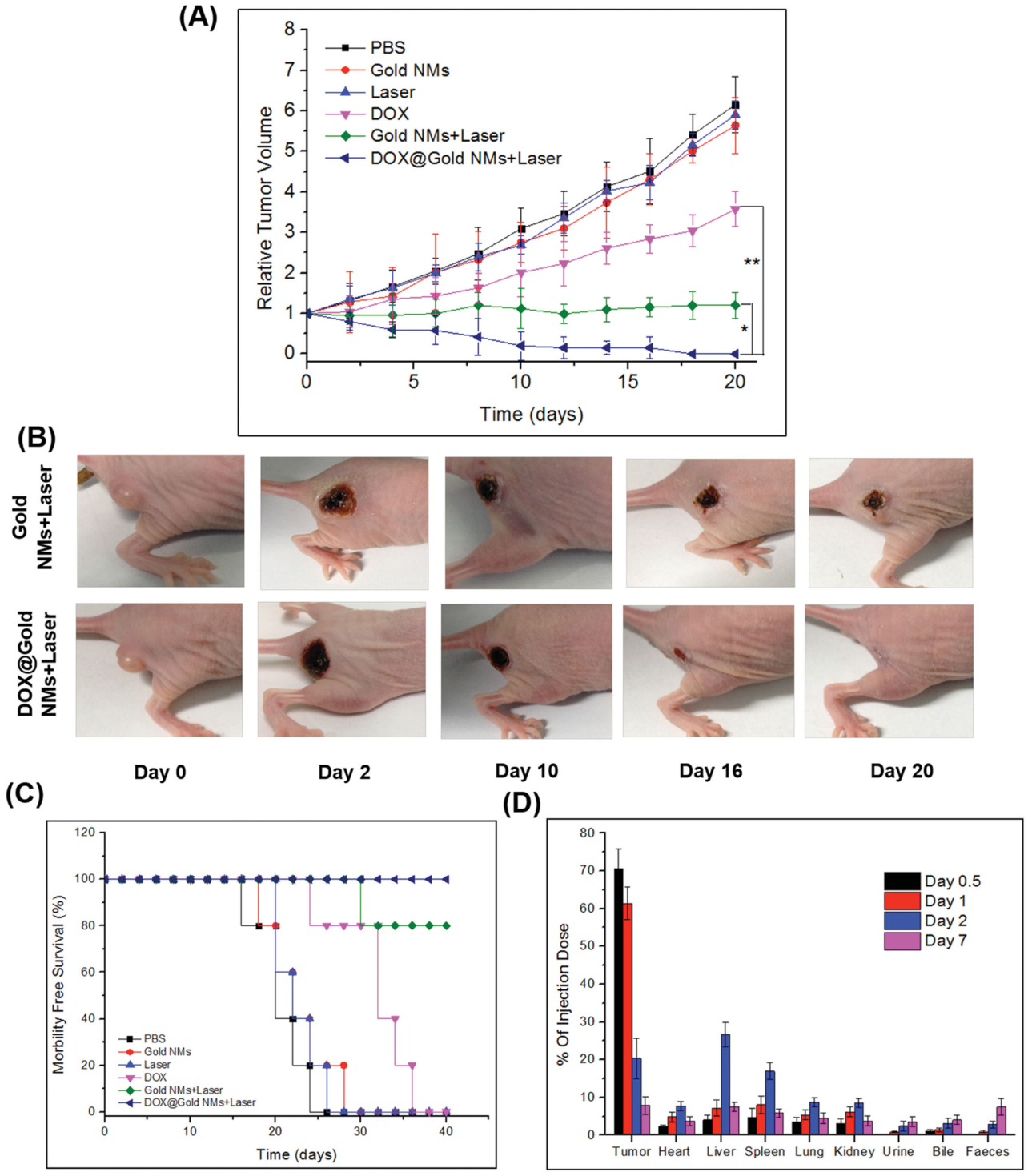

Figure 4. In vivo therapy experiment. A) Tumor growth curves of different groups of MCF-7 tumor-bearing mice after treatment (PBS, gold NMs only, Laser only, Dox only, gold NMs + laser, and DOX@gold NMs + laser). The tumor volumes were normalized to their initial sizes. The error bars represent the standard deviation of three mice per group. The free DOX group used an equivalent DOX concentration to the DOX@Gold NMs group. B) Representative pictures of mice after photothermal therapy and photothermal-chemotherapy. C) Survival curves of tumor-bearing mice after various treatments (five mice per group). D) The in vivo biodistributions of Au element after intratumoral injection of the gold NMs. $*P < 0.05$, $**P < 0.01$.

and photothermal therapy, our gold NMs offer a platform for more-effective combined photothermal-chemotherapy treatment, which shows a better cell-killing effect than either treatment alone. In vivo experiments further show a possibility that our gold NMs could be an effective contrast agent for CT imaging and PAT imaging at the same time. More importantly,

our gold NMs were assembled from 6 nm AuNPs, which would induce no potential toxicity; after finishing their theranostic duty, they would be dissociated into discrete AuNPs for clearance from the body. All in all, our first reported gold nanostructure constructed from novel comb-like amphipathic polymer opens new possibilities for assembling AuNPs for biomedical applications.

Experimental Section

Synthesis of p-(MEO_2MA_{270}-co-$HEMA_{260}$): *p*-(MEO_2MA_{270}-*co*-$HEMA_{260}$) was prepared via the RAFT method. In a typical procedure, 2-cyanoprop-2-yl-dithiobenzoate (10.4 mg, 0.05 mmol), monomer MEO_2MA (2.54 g, 13.5 mmol), HEMA (1.77 mg, 13.5 mmol), azodiisobutyronitrile (0.1 mg), and ethanol (5 mL) were added to a Schlenk tube sealed with a septum. After that, the tube was purged by dry nitrogen for half an hour. Then the mixture was heated at 60 °C in an oil bath under magnetic stirring for 12 h. The experiment was terminated by opening the flask. The final mixture was diluted in ethanol and then was followed by dialysis to remove the impurities and unreacted monomers. As an end, water was removed by lyophilization. In the same manner, copolymers of *p*-(MEO_2MA-*co*-HEMA) with different MEO_2MA/HEMA ratios were also synthesized.

Synthesis of p-(MEO_2MA_{270}-co-(HEMA-g-$PCL_{25})_{260}$): *p*-(MEO_2MA_{270}-*co*-(HEMA-*g*-$PCL_{25})_{260}$) was prepared by ring-opening polymerization using *p*-(MEO_2MA_{270}-*co*-$HEMA_{260}$) as initiator. In brief, a mixture of ε-caprolactone (8.7 g, 76.7 mmol), $Sn(Oct)_2$ (0.062 g, 0.153 mmol), as-synthesised *p*-(MEO_2MA_{270}-*co*-$HEMA_{260}$) (1 g, 0.0118 mmol), and toluene (10 mL) was added to a round-bottom flask with a condenser and a $CaCl_2$ drying tube. The mixture was maintained at 110 °C under strong stirring for 12 h. Then the reaction was stopped, and the mixture was precipitated from cold methanol. The precipitate was collected by filtration and dried in a desiccator to yield *p*-(MEO_2MA_{270}-*co*-(HEMA-*g*-$PCL_{25})_{260}$).

Multi-Mercapto-Terminated Polymer Synthesis: *p*-(MEO_2MA_{270}-*co*-(HEMA-*g*-$PCL_{25})_{260}$) (1 g), mercaptopropionic acid (60 mg), *N,N*-dicyclohexylcarbodiimide (120 mg), triethylamine (60 mg), and 4-(dimethylamino) pyridine (70 mg) were dissolved in anhydrous dichloromethane (120 mL), and the reaction was carried out for 24 h at room temperature under nitrogen. After evaporation of the solvent, the reactants were dissolved in dichloromethane and the urea byproduct was removed by filtration. Excess cold diethyl ether was added dropwise to the transparent solution to induce precipitation. The purified precipitates were isolated by filtration, lyophilized, and stored under vacuum for later use.

Synthesis and Self-Assembly of Gold NMs: Gold chains were synthesized by using $NaBH_4$ as a reductive agent in the presence of the comb-like polymer. In brief, $HAuCl_4$ (10 mg) and comb-like polymer (15 mg) was first dissolved in 5 mL of DMF. Then, 5 mL of DMF solution containing 10 mg of $NaBH_4$ were quickly added into the above solution under vigorous magnetic stirring. Subsequently, the mixture was stirred for 4 h followed by dilution with 10 mL of ethanol. The gold chain was further purified by centrifuged 3–4 times to remove unreacted polymer and redispersed in 5 mL of DMF. The self-assembly of gold chains was triggered by being dialyzed (dialysis bags with the MW cutoff of 3500 g mol^{-1}) against water for 12 h. To load DOX into gold NMs, 50 μL of a solution of DOX in DMF (2 mg mL^{-1}) were added into 5 mL of a solution of gold chains in DMF (2 mg mL^{-1}); then the mixed solution was dialyzed against water followed by being centrifuged to remove redundant DOX. To investigate the DOX release pattern under NIR light irradiation or not, 5 mg of DOX@Gold NMs were suspended in 2 mL of phosphate buffered saline (PBS) (10×10^{-4} M, pH 7.4), sealed in a dialysis bag and immersed in 20 mL of PBS, then exposed with or without NIR light. The amount of released DOX was monitored at regular time intervals. The release test was performed in triplicate to calculate a mean value and standard deviation.

Characterizations: The structures of polymer were examined by NMR (Bruker Avance 600 MHz, Bruker AXS Inc, Madison, Wisconsin). The morphology of the gold NMs was observed by transmission electron microscopy (TEM) (JEOL 2100F) at 200 kV. Thermogravimetric analysis (TGA) was carried out using a TG-209-F3 thermo gravimetric analyzer (Netzsch Instruments, Germany) with a heating rate of 10 °C min^{-1} from 30 to 700 °C in a N_2 atmosphere. UV–vis spectrophotometry measurements were performed on a TU-1810 UV–vis spectrophotometer (Persee, China) with a wavelength range from 400 to 1100 nm. ICP-MS measurements for gold materials were performed using an inductively coupled plasma mass spectrometer (Agilent 7500ce). The photothermal images were obtained by using a thermal camera (FLIR, T330) running on FLIR tools systems. In vivo CT imaging and PAT imaging were obtained by using Micro-CT system (Quantum FX, Caliper) and iTheraMedical MSOT.

Photothermal Treatment with NIR Light In Vitro: Human breast cancer cells (MCF-7) were purchased from Fuxiang Biotech Company, Shanghai, China) and cultured at 37 °C in a humidified atmosphere of 5% CO_2 and 95% air in high-glucose Dulbecco's modified Eagle medium (DMEM) containing 10% PBS and supplemented with penicillin (100 units mL^{-1}) and streptomycin (100 units mL^{-1}). For in vitro studies MCF-7 cells were incubated with 0.1 mg mL^{-1} gold NMs in a 96-well cell-culture plate at 37 °C and 5% CO_2. After the internalization of the gold NMs for 4 h and washing with PBS 3 times, the treated cells were irradiated by an 808 nm NIR laser at a power density of 1.5 W cm^{-2} for 5 min. A standard cell viability assay MTT was conducted to determine the cell killing efficiency after photothermal ablation. Cell viability was normalized to a control group without any treatment.

Photothermal Treatment with NIR Light In Vivo: All protocols for this animal study conformed to the Guide for the Care and Use of Laboratory Animals. In the in vivo studies, mice bearing MCF-7 tumors were intratumorally injected with 50 μL of 2 mg mL^{-1} gold NMs and then were irradiated with the 808 nm NIR laser at power density of 1.5 W cm^{-2} for 5 min. Real-time thermal imaging of MCF-7 tumors was monitored by FLIR. After treatment, the MCF-7 tumor volume was monitored. The tumor dimensions were determined at various time points using a caliper. The tumor volume (V) (mm^3) was calculated using the following formula: $V = ab^2/2$, where a is the length and b is the width in millimeters, respectively. The relative tumor volumes were calculated as V/V_0, where V_0 is the original tumor volume before the treatment was started. After the PTT, tumors were collected immediately for Hematoxylin and eosin staining.

Histopathology Assessments: Twenty days after the PTT, the animals were sacrificed and the main organs (heart, liver, spleen, lung, and kidney) were harvested and fixed in 10% neutral buffered formalin for 24 h, and then decalcified overnight, and processed through a gradient of alcohols then paraffin embedded. For hematoxylin-eosin staining, slides were immersed in the stain, washed, and mounted in *p*-xylene-bis-pyridiniumbromide (VWR, Dorset, UK) with obtained tissues section of 5 μm.

Acknowledgements

H.D. and F.D. contributed equally to this work. This work was financially supported by the National Natural Science Foundation of China (21304099, 51203162, 51103159, 51373177), the National High Technology Research and Development Program (2014AA020708, 2012AA022703, 2012AA020804), the Instrument Developing Project of the Chinese Academy of Sciences (YZ201253, YZ201313), the Open Funding Project of the National Key Laboratory of Biochemical Engineering (Y22504A169), the "Strategic Priority Research Program" of the Chinese Academy of Sciences (XDA09030301–3), and Beijing Natural Science Foundation (Grant no. Z141100000214010).

Received: March 25, 2015
Published online: May 6, 2015

[1] a) J. Chen, M. Yang, Q. Zhang, E. C. Cho, C. M. Cobley, C. Kim, C. Glaus, L. V. Wang, M. J. Welch, Y. Xia, *Adv. Funct. Mater.* **2010**, *20*, 3684; b) C. Wang, H. Xu, C. Liang, Y. Liu, Z. Li, G. Yang, L. Cheng, Y. Li, Z. Liu, *ACS Nano* **2013**, *7*, 6782; c) P. Huang, P. Rong, A. Jin, X. Yan, M. G. Zhang, J. Lin, H. Hu, Z. Wang, X. Yue, W. Li, G. Niu, W. Zeng, W. Wang, K. Zhou, X. Chen, *Adv. Mater.* **2014**, *26*, 6401; d) M. Zheng, S. Liu, J. Li, D. Qu, H. Zhao, X. Guan, X. Hu, Z. Xie, X. Jing, Z. Sun, *Adv. Mater.* **2014**, *26*, 3554; e) L. Cheng, J. Liu, X. Gu, H. Gong, X. Shi, T. Liu, C. Wang, X. Wang, G. Liu, H. Xing, *Adv. Mater.* **2014**, *26*, 1886.

[2] a) J. Lin, S. Wang, P. Huang, Z. Wang, S. Chen, G. Niu, W. Li, J. He, D. Cui, G. Lu, X. Chen, Z. Nie, *ACS Nano* **2013**, *7*, 5320; b) P. Huang, J. Lin, W. Li, P. Rong, Z. Wang, S. Wang, X. Wang, X. Sun, M. Aronova, G. Niu, R. D. Leapman, Z. Nie, X. Chen, *Angew. Chem. Int. Ed.* **2013**, *125*, 14208.

[3] H. Deng, Y. Zhong, M. Du, Q. Liu, Z. Fan, F. Dai, X. Zhang, *Theranostics* **2014**, *4*, 904.

[4] J. Song, J. Zhou, H. Duan, *J. Am. Chem. Soc.* **2012**, *134*, 13458.

[5] J. He, X. Huang, Y.-C. Li, Y. Liu, T. Babu, M. A. Aronova, S. Wang, Z. Lu, X. Chen, Z. Nie, *J. Am. Chem. Soc.* **2013**, *135*, 7974.

[6] Y.-S. Chen, Y.-C. Hung, I. Liau, G. S. Huang, *Nanoscale Res. Lett.* **2009**, *4*, 858.

[7] a) K. Yang, H. Xu, L. Cheng, C. Sun, J. Wang, Z. Liu, *Adv. Mater.* **2012**, *24*, 5586; b) K. C. Hribar, M. H. Lee, D. Lee, J. A. Burdick, *ACS Nano* **2011**, *5*, 2948.

[8] S. K. Ghosh, T. Pal, *Chem. Rev.* **2007**, *107*, 4797.

[9] H. Shi, Y. Zhao, X. Dong, Y. Zhou, D. Wang, *Chem. Soc. Rev.* **2013**, *42*, 2075.

[10] a) J. H. Yang, P. Zhang, L. Tang, P. Sun, W. G. Liu, P. Sun, A. J. Zuo, D. C. Liang, *Biomaterials* **2010**, *31*, 144; b) G. Z. Gu, H. M. Xia, Q. Y. Hu, Z. Y. Liu, M. Y. Jiang, T. Kang, D. Y. Miao, Y. F. Tu, Z. Q. Pang, Q. X. Song, L. Yao, H. Z. Chen, X. L. Gao, J. Chen, *Biomaterials* **2013**, *34*, 196.

[11] a) J.-F. Lutz, O. Akdemir, A. Hoth, *J. Am. Chem. Soc.* **2006**, *128*, 13046; b) J. T. Wiltshire, G. G. Qiao, *Macromolecules* **2008**, *41*, 623.

[12] E. Kim, J. Yang, J. Choi, J. S. Suh, Y. M. Huh, S. Haam, *Nanotechnology* **2009**, 20.

[13] a) N. R. Jana, L. Gearheart, C. J. Murphy, *Adv. Mater.* **2001**, *13*, 1389; b) M. C. Daniel, D. Astruc, *Chem. Rev.* **2004**, *104*, 293.

[14] J. B. Song, L. Cheng, A. P. Liu, J. Yin, M. Kuang, H. W. Duan, *J. Am. Chem. Soc.* **2011**, *133*, 10760.

[15] J. You, G. D. Zhang, C. Li, *ACS Nano* **2010**, *4*, 1033.

[16] a) Z. Zhang, L. Wang, J. Wang, X. Jiang, X. Li, Z. Hu, Y. Ji, X. Wu, C. Chen, *Adv. Mater.* **2012**, *24*, 1418; b) Y. Ma, X. Liang, S. Tong, G. Bao, Q. Ren, Z. Dai, *Adv. Funct. Mater.* **2013**, *23*, 815; c) M. Liu, Z. Wang, S. Zong, H. Chen, D. Zhu, Y. Zhong, Y. Cui, *J. Biomed. Nanotechnol.* **2015**, *11*, 979; d) Y.-Y. Bai, S. Zheng, L. Zhang, K. Xia, X. Gao, Z.-H. Li, C. Li, N. He, S. Ju, *J. Biomed. Nanotechnol.* **2014**, *10*, 3351; e) A. M. Pekkanen, M. R. DeWitt, M. N. Rylander, *J. Biomed. Nanotechnol.* **2014**, *10*, 1677; f) P. Prabhu, V. Patravale, *J. Biomed. Nanotechnol.* **2012**, *8*, 859; g) J. Peng, T. Qi, J. Liao, B. Chu, Q. Yang, Y. Qu, W. Li, H. Li, F. Luo, Z. Qian, *Theranostics* **2014**, *4*, 678.

[17] C.-L. Peng, Y.-H. Shih, P.-C. Lee, T. M.-H. Hsieh, T.-Y. Luo, M.-J. Shieh, *ACS Nano* **2011**, *5*, 5594.

[18] a) D. Kim, S. Park, J. H. Lee, Y. Y. Jeong, S. Jon, *J. Am. Chem. Soc.* **2007**, *129*, 7661; b) L. V. Wang, *Nat. Photonics* **2009**, *3*, 503; c) D. Kim, Y. Y. Jeong, S. Jon, *ACS Nano* **2010**, *4*, 3689; d) X. Wang, Y. Pang, G. Ku, X. Xie, G. Stoica, L. V. Wang, *Nat. Biotechnol.* **2003**, *21*, 803.

[19] P. Huang, L. Bao, C. Zhang, J. Lin, T. Luo, D. Yang, M. He, Z. Li, G. Gao, B. Gao, S. Fu, D. Cui, *Biomaterials* **2011**, *32*, 9796.

[20] a) S. Mitragotri, J. Lahann, *Nat. Mater.* **2009**, *8*, 15; b) A. E. Nel, L. Madler, D. Velegol, T. Xia, E. M. V. Hoek, P. Somasundaran, F. Klaessig, V. Castranova, M. Thompson, *Nat. Mater.* **2009**, *8*, 543.